



# THE CRITICAL MASS RATIO OF DOUBLE WHITE DWARF BINARIES FOR VIOLENT MERGER-INDUCED TYPE IA SUPERNOVA EXPLOSIONS

YUSHI SATO<sup>1,2</sup>, NAOHITO NAKASATO<sup>3</sup>, ATARU TANIKAWA<sup>2,4</sup>, KEN'ICHI NOMOTO<sup>5,7</sup>, KEIICHI MAEDA<sup>6,5</sup>, AND IZUMI HACHISU<sup>2</sup>

<sup>1</sup>Department of Astronomy, Graduate School of Science, The University of Tokyo, 7-3-1 Hongo, Bunkyo-ku, Tokyo 113-0033, Japan; [sato@ea.c.u-tokyo.ac.jp](mailto:sato@ea.c.u-tokyo.ac.jp)

<sup>2</sup>Department of Earth Science and Astronomy, College of Arts and Sciences, The University of Tokyo, 3-8-1 Komaba, Meguro-ku, Tokyo 153-8902, Japan

<sup>3</sup>Department of Computer Science and Engineering, University of Aizu, Tsuruga Ikki-machi Aizu-Wakamatsu, Fukushima 965-8580, Japan

<sup>4</sup>RIKEN Advanced Institute for Computational Science, 7-1-26 Minatojima-minami-machi, Chuo-ku, Kobe, Hyogo 650-0047, Japan

<sup>5</sup>Kavli Institute for the Physics and Mathematics of the universe (WPI), The University of Tokyo, 5-1-5 Kashiwanoha, Kashiwa, Chiba 277-8583, Japan

<sup>6</sup>Department of Astronomy, Kyoto University, Kitashirakawa-Oiwake-cho, Sakyo-ku, Kyoto 606-8502, Japan

Received 2015 September 10; accepted 2016 March 2; published 2016 April 11

## ABSTRACT

Mergers of carbon–oxygen (CO) white dwarfs (WDs) are considered to be one of the potential progenitors of type Ia supernovae (SNe Ia). Recent hydrodynamical simulations showed that the less massive (secondary) WD violently accretes onto the more massive (primary) one, carbon detonation occurs, the detonation wave propagates through the primary, and the primary finally explodes as a sub-Chandrasekhar mass SN Ia. Such an explosion mechanism is called the violent merger scenario. Based on the smoothed particle hydrodynamics simulations of merging CO WDs, we derived a critical mass ratio ( $q_{\text{cr}}$ ) leading to the violent merger scenario that is more stringent than previous results. We conclude that this difference mainly comes from the differences in the initial condition of whether or not the WDs are synchronously spinning. Using our new results, we estimated the brightness distribution of SNe Ia in the violent merger scenario and compared it with previous studies. We found that our new  $q_{\text{cr}}$  does not significantly affect the brightness distribution. We present the direct outcome immediately following CO WD mergers for various primary masses and mass ratios. We also discussed the final fate of the central system of the bipolar planetary nebula Henize 2-428, which was recently suggested to be a double CO WD system whose total mass exceeds the Chandrasekhar-limiting mass, merging within the Hubble time. Even considering the uncertainties in the proposed binary parameters, we concluded that the final fate of this system is almost certainly a sub-Chandrasekhar mass SN Ia in the violent merger scenario.

**Key words:** binaries: close – galaxies: evolution – hydrodynamics – supernovae: general – white dwarfs

## 1. INTRODUCTION

SNe Ia have been considered to be thermonuclear explosions of a CO white dwarf (WD). They play important roles in astronomy as a standard candle to determine the cosmological parameters (e.g., Riess et al. 1998; Perlmutter et al. 1999) and as major sources of iron group elements (e.g., Kobayashi et al. 1998). However, their progenitor systems and explosion mechanisms are still uncertain (e.g., Hillebrandt & Niemeyer 2000; Maoz et al. 2014). A merger of CO WDs has been considered as one of the potential progenitors of SNe Ia, which is called the double degenerate (DD) scenario (Iben & Tutukov 1984; Webbink 1984). A binary of CO WDs loses its angular momentum by emitting gravitational waves and finally merges. When the total mass exceeds the critical mass ( $M_{\text{ig}} = 1.38 M_{\odot}$ , Nomoto et al. 1984) for the carbon ignition in the center, such a system has been proposed to give rise to an SN Ia explosion. Some observational studies reported that neither surviving companions (e.g., González Hernández et al. 2012; Kerzendorf et al. 2012; Schaefer & Pagnotta 2012) nor signatures of them (e.g., Brown et al. 2012; Foley et al. 2012; Olling et al. 2015) were detected in some well studied SN Ia remnants and nearby SNe Ia, but recently there have been several examples which possibly show these signatures as well both in SNe with special properties (McCully et al. 2014; Cao et al. 2015) and in a normal SN Ia (Marion et al. 2015). These studies suggest that at least a part of SNe Ia would originate from either the DD scenario or the  $J$ (angular

momentum)-loss induced “delayed” carbon ignition in the single degenerate scenario (e.g., Benvenuto et al. 2015).

After Benz et al. (1990) first performed three-dimensional (3D) hydrodynamical simulations of CO WD mergers with their smoothed particle hydrodynamics (SPH) code (e.g., Gingold & Monaghan 1982; Monaghan 2005; Rosswog 2009), similar merger simulations have been performed by various groups (e.g., Rasio & Shapiro 1995; Segretain et al. 1997; Guerrero et al. 2004; D’Souza et al. 2006; Motl et al. 2007; Yoon et al. 2007; Lorén-Aguilar et al. 2009; Fryer et al. 2010; Pakmor et al. 2010, 2011, 2012a, 2012b; Dan et al. 2011, 2012, 2014; Raskin et al. 2012, 2014; Zhu et al. 2013; Moll et al. 2014; Kashyap et al. 2015; Sato et al. 2015; Tanikawa et al. 2015). These studies showed that a CO WD merger could lead to an SN Ia if several conditions are satisfied. Pakmor et al. (2010, 2011, 2012a, 2012b) simulated mergers of CO WDs (both of the binary members have masses  $\sim 1 M_{\odot}$ ) with their SPH code. They found that the secondary WD violently accreted onto the primary and carbon detonation would occur during the merger. They showed that a detonation wave propagated through the primary and the primary finally exploded as an SN Ia. They called this explosion mechanism “the violent merger scenario.” As the mass ratio  $q \equiv M_2/M_1$ , where  $M_1$  is the primary mass and  $M_2$  is the secondary mass, approaches unity, the mass accretion becomes more violent and the carbon detonation occurs more easily. Therefore, the mass ratio is an important parameter for the violent merger scenario.

Pakmor et al. (2011) investigated the critical mass ratio  $q_{\text{cr}}$ , above which the violent merger scenario is realized, and found that  $q_{\text{cr}} \sim 0.8$  for  $M_1 = 0.9 M_{\odot}$ . Dan et al. (2012)

<sup>7</sup> Hamamatsu Professor.

studied mergers of WDs over a wide range of masses, i.e.,  $0.2 \sim 1.2 M_{\odot}$ . They found that dynamical carbon burning did not occur in all of their models. However, their numerical resolution was low ( $\sim 20,000$  particles per star). Sato et al. (2015) performed SPH simulations of CO WD mergers over a wide range of masses ( $0.5 \sim 1.1 M_{\odot}$ ) and with a resolution of 500,000 particles per  $M_{\odot}$ , i.e.,  $500,000 M_{\odot}^{-1}$ . They investigated whether or not dynamical carbon burning would occur during the merger. Pakmor et al. (2012a) and Sato et al. (2015) showed that the numerical resolution is another important factor in studying the violent merger scenario, and Sato et al. (2015) suggested that it should be  $\geq 500,000 M_{\odot}^{-1}$  (see also Tanikawa et al. 2015).

Assuming critical mass ratios for the violent merger scenario based on the result of Pakmor et al. (2011), Ruiter et al. (2013) estimated the brightness distribution of SNe Ia and suggested that it could be qualitatively consistent with what is observed (Li et al. 2011). Because the critical mass ratio could have influence on the distribution of SN Ia brightness, a detailed investigation of the critical mass ratio is required to verify the violent merger scenario.

Recently, Santander-García et al. (2015) reported that the central system of the bipolar planetary nebula (PN) Henize 2-428 might be a super-Chandrasekhar DD pair. They estimated the combined mass as  $\sim 1.8 M_{\odot}$  and the mass ratio as  $\sim 1$ . Although there are some negative arguments against their conclusion (e.g., Frew et al. 2015; Garcia-Berro et al. 2015), Henize 2-428 is a candidate progenitor for the violent merger scenario, if the interpretation by Santander-García et al. (2015) is correct. While Sato et al. (2015) have already simulated a set of primary and secondary masses which cover a plausible parameter space for Henize 2-428, their mass grids were too coarse. In this paper, we perform some additional (much finer grids of the masses) SPH simulations of CO WD mergers to accurately obtain the critical mass ratio for the violent merger scenario. We try to derive the relation between  $M_1$  and  $q_{\text{cr}}$ , and compare it with previous studies. We also use our results to discuss the final fate of Henize 2-428.

This paper is organized as follows. In Section 2, we briefly describe our numerical method. Our results are shown in Section 3 and we discuss them in Section 4. We summarize our findings in Section 5.

## 2. NUMERICAL METHODS

Our SPH simulations of CO WD mergers are essentially the same as those of Sato et al. (2015). We used the OcTree On OpenCL code, which was developed for various particle simulations for astrophysical fluid phenomena (Nakasato et al. 2012). The equation of state (EOS) is that of Timmes & Swesty (2000). Initial setups are also the same as those in Sato et al. (2015), which refer to Rasio & Shapiro (1995) and Dan et al. (2011). Our CO WD models have a uniform composition of 50% carbon and 50% oxygen in mass. Sato et al. (2015) simulated mergers of CO WDs whose masses were 0.5, 0.6, 0.7, 0.8, 0.9, 1.0, and  $1.1 M_{\odot}$ .

In this paper, we performed additional simulations of CO WD mergers to accurately determine the critical mass ratio  $q_{\text{cr}}$  to realize the violent merger scenario. We add  $M_2 = 0.725, 0.75, 0.775, 0.825, 0.85$ , and  $0.875 M_{\odot}$  for each  $M_1 = 0.75, 0.8, 0.9, 1.0$ , and  $1.1 M_{\odot}$ , because  $q_{\text{cr}}$  seems to be in this mass range (see Figure 5 of Sato et al. 2015). The numerical resolution is 500  $k$  per solar mass ( $k \equiv 1,024$ ). Our

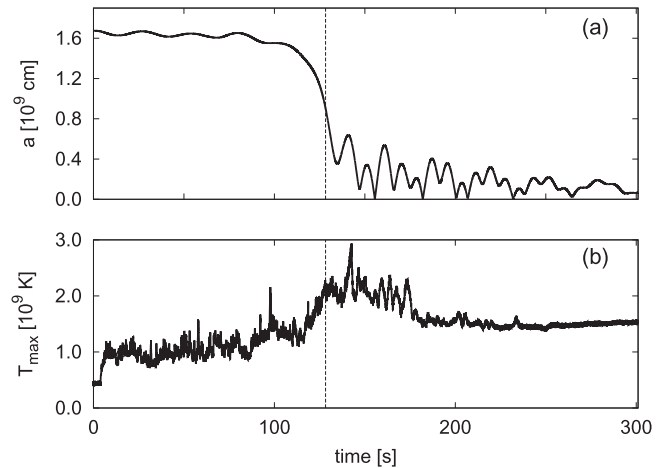


**Figure 1.** Time evolutions of (a) the orbital separation and (b) the maximum temperature in the case of  $1.1 + 0.9 M_{\odot}$ . Vertical dashed lines show the time when the first detonating particle appears.

SPH scheme derives the temperature of a particle from the density and internal energy through the EOS. The estimations of density and internal energy have some numerical noises, and the derived temperature is also fluctuated (Dan et al. 2012; Sato et al. 2015; Tanikawa et al. 2015).

Because the nuclear burning rate is sensitive to temperature, it might strongly enhance the fluctuated temperature. Therefore, we first performed our simulations without nuclear reactions, as in our previous work (Sato et al. 2015), and determined the critical mass ratio for the violent merger scenario. Then, we added simulations including nuclear reactions in order to confirm that the inclusion of nuclear burning in our SPH simulation increases the temperature high enough to really satisfy the detonation condition for the models above the critical mass ratio (see Section 4.3).

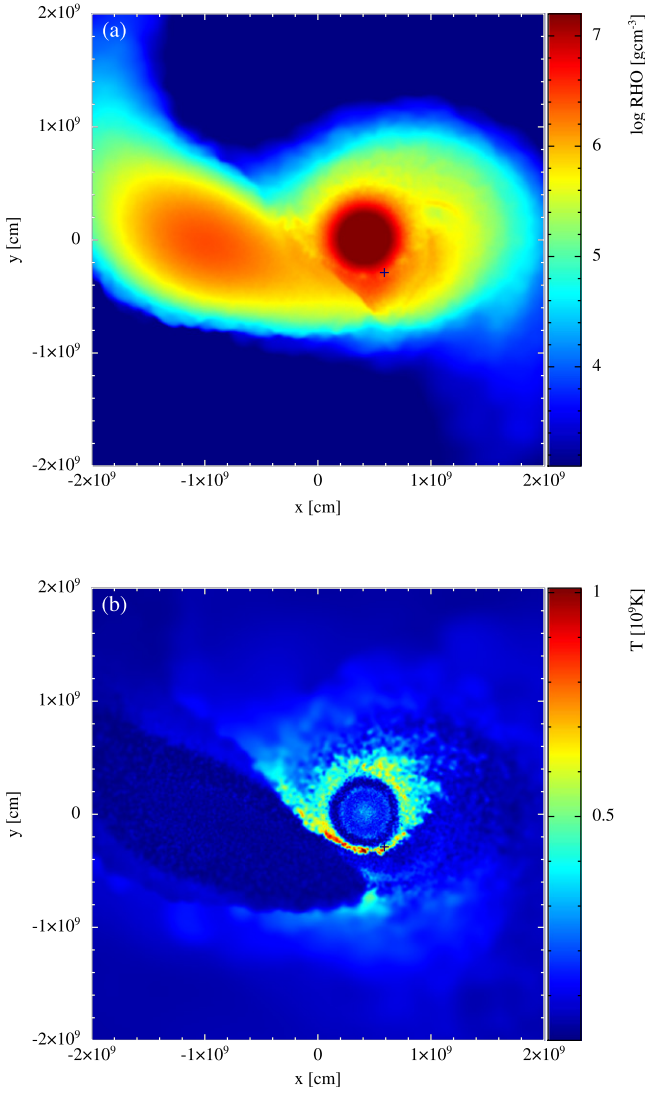
## 3. RESULTS

Figure 1 shows the time evolution of the orbital separation and the maximum temperature in the case of  $1.1 + 0.9 M_{\odot}$ . They indicate that the temperature increases drastically when the secondary is completely disrupted and accretes onto the primary, which is consistent with previous studies. Black vertical dashed lines show the time when our detonation condition, which is described below in Section 3.1, is first fulfilled. Figure 2 depicts the density and temperature profiles of the equatorial plane at the time which is indicated by the black dashed lines in Figure 1. The profile and morphology are consistent with the similar cases in Pakmor et al. (2012a, 2012b).

Figure 3 shows the density and temperature of the particle with the smallest  $\tau_{\text{CC}}/\tau_{\text{dyn}}$  ratio in each merger simulation, where  $\tau_{\text{CC}}$  and  $\tau_{\text{dyn}}$  are carbon burning and dynamical timescales, respectively, as defined below. The colors and shapes of the symbols indicate the total mass,  $M_{\text{tot}} = M_1 + M_2$ , and the primary mass,  $M_1$ , respectively. A black solid line shows the line of  $\tau_{\text{CC}}/\tau_{\text{dyn}} = 1$ .

### 3.1. Conditions for Violent Merger-induced Explosions

For the violent merger scenario, it is crucial to know whether or not carbon detonation occurs during a merger. Although Pakmor et al. (2011) used the results of Seitenzahl et al. (2009)



**Figure 2.** (a) Density and (b) temperature profiles on the equatorial plane at the time of dashed line in Figure 1. A black cross indicates the first detonating particle.

as the detonation condition, the treatment is still controversial. In this paper, we judge it from the condition of whether it triggers the dynamical carbon burning. We obtain the dynamical timescale (e.g., Nomoto 1982),

$$\tau_{\text{dyn}} = \frac{1}{\sqrt{24\pi G\rho}}, \quad (1)$$

and the carbon burning timescale,

$$\tau_{\text{CC}} = \frac{C_p T}{\epsilon_{\text{CC}}}, \quad (2)$$

for each SPH particle. Here,  $\rho$  and  $T$  are the particle's density and temperature, respectively,  $C_p$  is the specific heat at the constant pressure of a particle,  $G$  is the gravitational constant, and  $\epsilon_{\text{CC}}$  is the energy generation rate of carbon burning (see Equation (6) of Sato et al. 2015). When there are any particles that satisfy  $\tau_{\text{CC}} < \tau_{\text{dyn}}$ , carbon ignites dynamically. We regard this as the detonation condition.

If  $\tau_{\text{CC}} < \tau_{\text{dyn}}$ , the temperature increases more rapidly than it decreases by adiabatic expansion and accelerates carbon

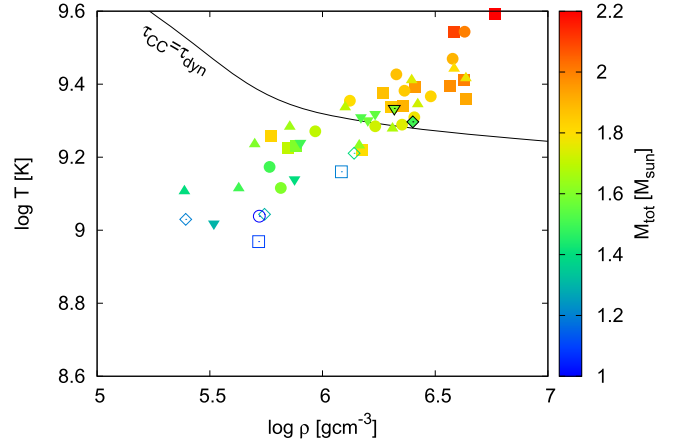


**Figure 3.** Density and temperature of a particle with the smallest  $\tau_{\text{CC}}/\tau_{\text{dyn}}$  ratio for each CO WD merger model. The colors of the symbols indicate the total mass of the system. The shapes of symbols indicate the mass of the primary. The filled squares are the  $1.1 M_{\odot}$  primary, the filled circles  $1.0 M_{\odot}$ , the filled triangles  $0.9 M_{\odot}$ , the filled inverted triangles  $0.8 M_{\odot}$ , the filled diamonds  $0.75 M_{\odot}$ , the open diamonds  $0.7 M_{\odot}$ , the open squares  $0.6 M_{\odot}$ , and the open circles  $0.5 M_{\odot}$ . The symbols surrounded by black frames indicate  $0.8 + 0.8 M_{\odot}$  (filled inverted triangle) and  $0.75 + 0.75 M_{\odot}$  (filled diamond), respectively. A black solid line indicates  $\tau_{\text{CC}} = \tau_{\text{dyn}}$ .

burning. The temperature would increase high enough to satisfy the detonation condition, such as the results of Seitenzahl et al. (2009). Thus, we consider that the condition of the dynamical carbon burning ( $\tau_{\text{CC}} < \tau_{\text{dyn}}$ ) is a plausible detonation condition in the case without nuclear reactions. We confirm this later by including carbon burning in our SPH code in Section 4.3.

As described in Section 2, temperature is possibly affected by numerical noises in our SPH simulations. In order to minimize the influence of temperature noise in judging the condition for carbon detonation, we examine whether the particle continuously satisfies the above condition for at least a dynamical timescale ( $\tau_{\text{dyn}} \sim 0.4$  s at  $\rho \sim 10^6$  g cm $^{-3}$ ). If so, we assume that dynamical carbon burning is definitely initiated and detonation occurs. For example, mergers of  $0.8 + 0.8 M_{\odot}$  and  $0.75 + 0.75 M_{\odot}$ , which are surrounded by black frames in Figure 3, both satisfy  $\tau_{\text{CC}} < \tau_{\text{dyn}}$ . However, in the case of  $0.75 + 0.75 M_{\odot}$ , there are no particles which continuously satisfy the above condition for a dynamical timescale. We thus regard that detonation does not occur in the merger of  $0.75 + 0.75 M_{\odot}$ . In the case of  $0.8 + 0.8 M_{\odot}$ , on the other hand, three particles keep  $\tau_{\text{CC}} < \tau_{\text{dyn}}$  for longer than  $\tau_{\text{dyn}}$ . Therefore, we consider that carbon detonation does occur in the case of  $0.8 + 0.8 M_{\odot}$  and eventually the system leads to an SN Ia in the violent merger scenario.

### 3.2. The Critical Mass Ratio for Violent Merger Scenarios

We plot our numerical results of a violent merger scenario in Figure 4. Here, the filled circles denote models which satisfy our condition for carbon detonation while the crosses denote the models which do not. The black dashed line indicates  $M_1 = M_2$ . Figure 4 shows that carbon detonation occurs only in the models whose primary and secondary masses are more massive than  $\sim 0.8 M_{\odot}$ , which is consistent with the results of Sato et al. (2015).

We derived approximate formulae of the critical mass ratio,  $q_{\text{cr}}$ , as a function of the primary mass,  $M_1$ , and plot them in Figure 5, both of which are on logarithmic scales. The red solid

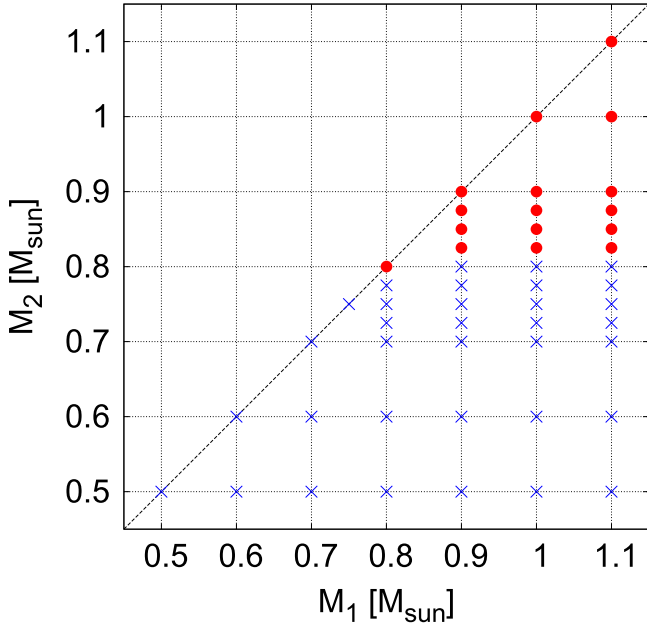


**Figure 4.** Filled circles indicate the mass combinations which satisfy our condition for carbon detonation while crosses indicate those which do not satisfy the condition. A black dashed line is where the mass ratio equals unity.

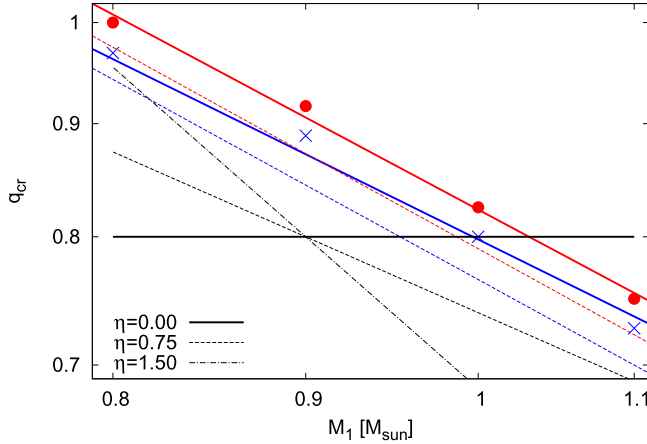


**Figure 5.** Critical mass ratio for the violent merger scenario as a function of the primary mass. A red solid line denotes an upper bound represented by Equation (3), while a blue solid line shows a lower bound represented by Equation (4). We also present the results including carbon burning. The red and blue dashed lines correspond to the upper and lower bounds, respectively, for the violent merger scenario in the case with carbon burning. The critical mass ratios adopted by Ruiter et al. (2013) are also depicted by a black solid, dashed, and dashed-dotted lines. See the text for more details.

line is for an upper bound, while the blue solid line is for a lower bound. They are represented by

$$q_{\text{cr}} = 0.82 \left( \frac{M_1}{M_{\odot}} \right)^{-0.91} \quad (\text{upper bound}), \quad (3)$$

$$q_{\text{cr}} = 0.80 \left( \frac{M_1}{M_{\odot}} \right)^{-0.84} \quad (\text{lower bound}), \quad (4)$$

respectively. Considering the lowest mass ratios in which the model satisfies our condition for carbon detonation, we derive Equation (3). On the other hand, we derive Equation (4) from

the highest mass ratios in which the model does not satisfy our condition for carbon detonation.

If a sizable helium layer exists on the CO WD, helium detonation could occur during a merger and induce carbon detonation (e.g., Guillochon et al. 2010; Dan et al. 2012; Raskin et al. 2012; Pakmor et al. 2013; Tanikawa et al. 2015). In this helium-ignited violent merger scenario,  $q_{\text{cr}}$  could be smaller than Equations (3) and (4). However, such a study needs a much finer resolution because the occurrence of helium detonation depends strongly on the mass of the helium layer (e.g., Tanikawa et al. 2015). We leave such a systematic study to our future work.

## 4. DISCUSSION

### 4.1. Comparison with Previous Studies

Pakmor et al. (2011) obtained  $q_{\text{cr}} \sim 0.8$  for  $M_1 = 0.9 M_{\odot}$ . Our results show a different value of  $q_{\text{cr}} \sim 0.9$  for  $M_1 = 0.9 M_{\odot}$ . This discrepancy could arise from the differences in (1) the initial conditions, (2) numerical resolution, and (3) inclusion of nuclear burning. We discuss these three effects in this order.

Pakmor et al. (2011) used non-spinning WDs and set them at the initial separation where the Roche lobe overflow (RLOF) just started in the sense of Eggleton's (1983) approximation. On the other hand, we assume that the WDs spin synchronously with the orbital motion, and set them at an initial separation large enough to avoid the RLOF. We decrease the separation until the RLOF starts (Rasio & Shapiro 1995; Dan et al. 2011; Sato et al. 2015). For the initial condition of Pakmor et al. (2011), as mentioned in Dan et al. (2011), the secondary accretes onto the primary more violently than for the case of synchronously spinning WDs. As a result, carbon detonation would occur easily. We examined the merger of  $0.9 + 0.75 M_{\odot}$  WDs in an initial condition similar to that of Pakmor et al. (2011). We thereby found that there exist 16 particles which satisfy the condition for carbon detonation in this case, while there is no such particle for our initial condition (see Figure 3). Although no definite conclusion has yet been reached, several numerical studies suggest that compact WD binaries would reach synchronization before their merging due to angular momentum dissipation by tidally excited gravity waves (e.g., Fuller & Lai 2014, and references therein).

### 4.2. Numerical Resolution

Numerical resolution might also cause the difference. Sato et al. (2015) reported that the maximum temperature and the minimum  $\tau_{\text{CC}}/\tau_{\text{dyn}}$  ratio did not converge in the range of  $10k \sim 500k M_{\odot}^{-1}$ . This is because smaller hot regions can be resolved as the numerical resolution becomes higher. Several previous studies also indicated that numerical resolution would affect their results (e.g., Pakmor et al. 2011, 2012a). In this paper, we performed several simulations with numerical resolutions higher ( $1000k M_{\odot}^{-1}$ ,  $2000k M_{\odot}^{-1}$ ) than our standard ones ( $500k M_{\odot}^{-1}$ ) for  $0.8 + 0.775 M_{\odot}$ ,  $0.9 + 0.8 M_{\odot}$ , and  $1.1 + 0.8 M_{\odot}$  WDs. Our numerical results are summarized in Figure 6. The maximum temperature still increases and the minimum  $\tau_{\text{CC}}/\tau_{\text{dyn}}$  ratio decreases except for  $0.8 + 0.775 M_{\odot}$  as the numerical resolution increases. Similar trends were also reported in Pakmor et al. (2012a), Sato et al. (2015), and Tanikawa et al. (2015). These trends indicate that our numerical results have not yet been fully converged. Therefore,



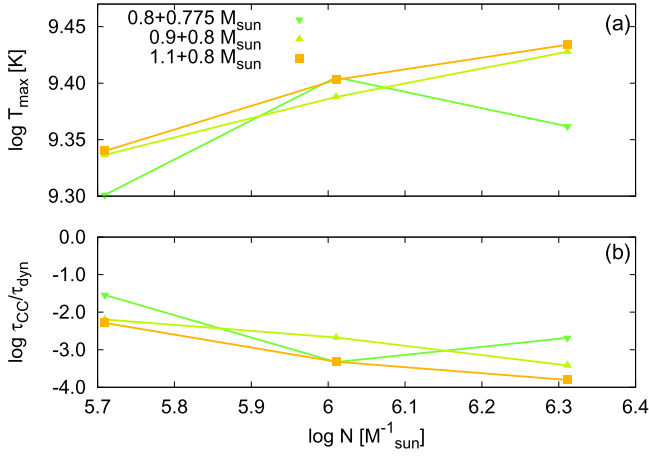


**Figure 6.** Dependence of (a) the maximum temperature and (b) the minimum  $\tau_{CC}/\tau_{dyn}$  ratio on the numerical resolution. The horizontal axis is the number of SPH particles per solar mass. The shapes and colors of the symbols have the same meanings as those in Figure 3.

our critical mass ratio could be slightly lower than the red solid line in Figure 5.

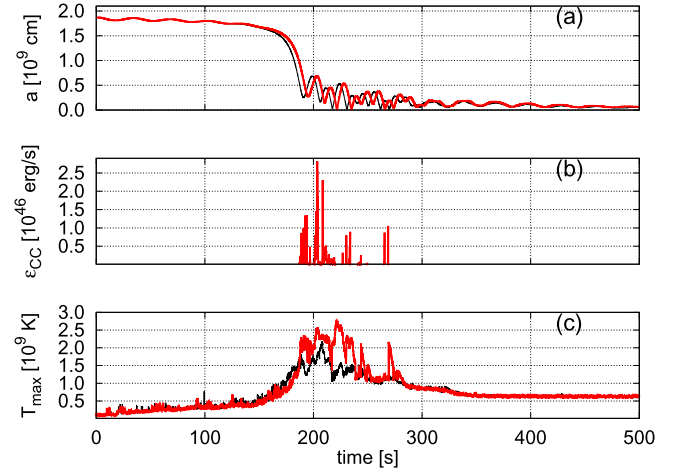
#### 4.3. The Effect of Nuclear Burning

The inclusion of nuclear reactions could also make a difference between the results of Pakmor et al. (2011) and our results. Pakmor et al. (2011) found that particles with high temperature ( $\geq 2 \times 10^9$  K) did not exist in the case of  $0.9 + 0.81 M_\odot$  without nuclear reactions. On the other hand, they existed in the case with nuclear reactions.

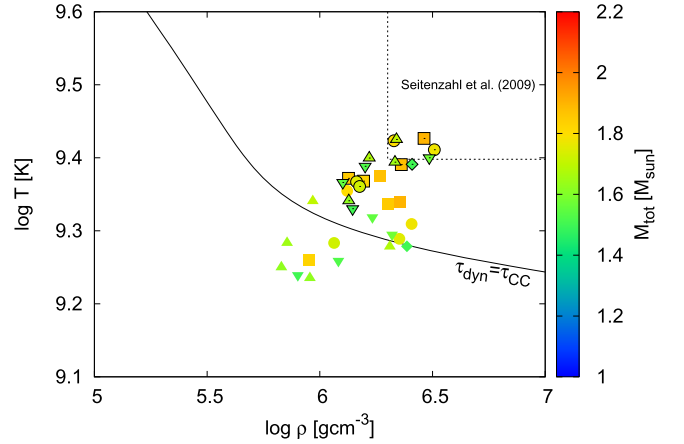
In order to evaluate the effect of nuclear energy release, we performed additional simulations, including nuclear burning, for some models. In these simulations, we include only carbon burning, i.e.,  $^{12}\text{C} + ^{12}\text{C}$  reaction, to avoid the large computational cost for solving a reaction network. The formulation of the reaction rate is the same as Equation (6) of our previous work (Sato et al. 2015). Because the initiation of carbon detonation is judged by this reaction, such a simple treatment of nuclear reactions would be sufficient for our purpose. The electron screening effect is negligibly small in the region of  $\rho = 10^6\text{--}10^7 \text{ g cm}^{-3}$  and  $T > 2 \times 10^9$  K, where carbon detonation would occur, so we do not include this effect.

Figure 7 shows the comparison between simulations with and without carbon burning for the case of  $0.9 + 0.8 M_\odot$ . The red lines indicate the case with carbon burning, while the black ones indicate the case without. Although the orbital evolution (Figure 7(a)) is almost the same, the maximum temperature (Figure 7(c)) realized in the case with carbon burning is higher than the case without during the merger phase. This difference comes from the nuclear energy release (Figure 7(b)). We confirmed that the inclusion of carbon burning increases the maximum temperature. Figure 8 summarizes the density and temperature of a particle which has the smallest  $\tau_{CC}/\tau_{dyn}$  ratio for all the cases we recalculated, including nuclear burning. The symbols surrounded by black frames are the results of the cases with carbon burning.

Since our simulations include only carbon burning, the effect of nuclear reactions would be underestimated. To check this effect, we perform post-processing calculations using an  $\alpha$ -chain reaction network containing 13 species from  $^4\text{He}$  to  $^{56}\text{Ni}$  (Timmes 1999). Figure 9 shows the results for a



**Figure 7.** Merger of  $0.9 + 0.8 M_\odot$  WDs. The red lines indicate the case with carbon burning, while the black lines indicate the case without. (a) The orbital evolution, (b) the energy release rate of carbon burning, and (c) the time evolution of maximum temperature.



**Figure 8.** Same as Figure 3, but for the case with carbon burning. The symbols surrounded by black frames are the case with carbon burning while those without black frames are the case without. The black dashed line is the demarcation of the detonation condition by Seitenzahl et al. (2009).

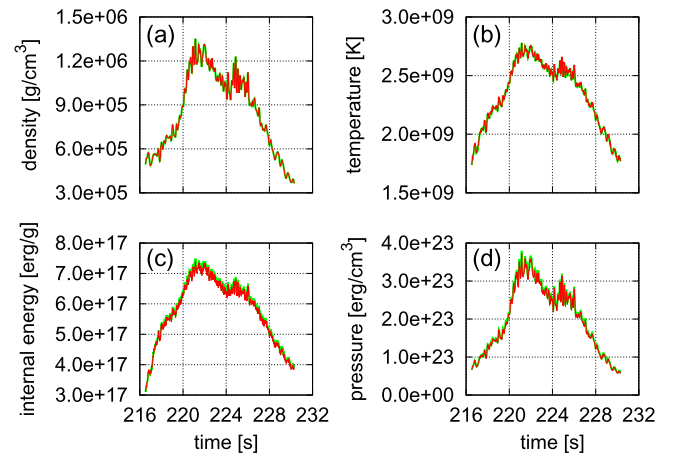


**Figure 9.** Post-processing analysis in the case of  $0.9 + 0.8 M_\odot$ . We have calculated nuclear energy generation using the 13 species  $\alpha$ -chain reaction network (Timmes 1999). Green lines denote the case of only carbon burning while the red lines indicate those of post-processing results. (a) Density, (b) temperature, (c) specific internal energy, and (d) pressure.

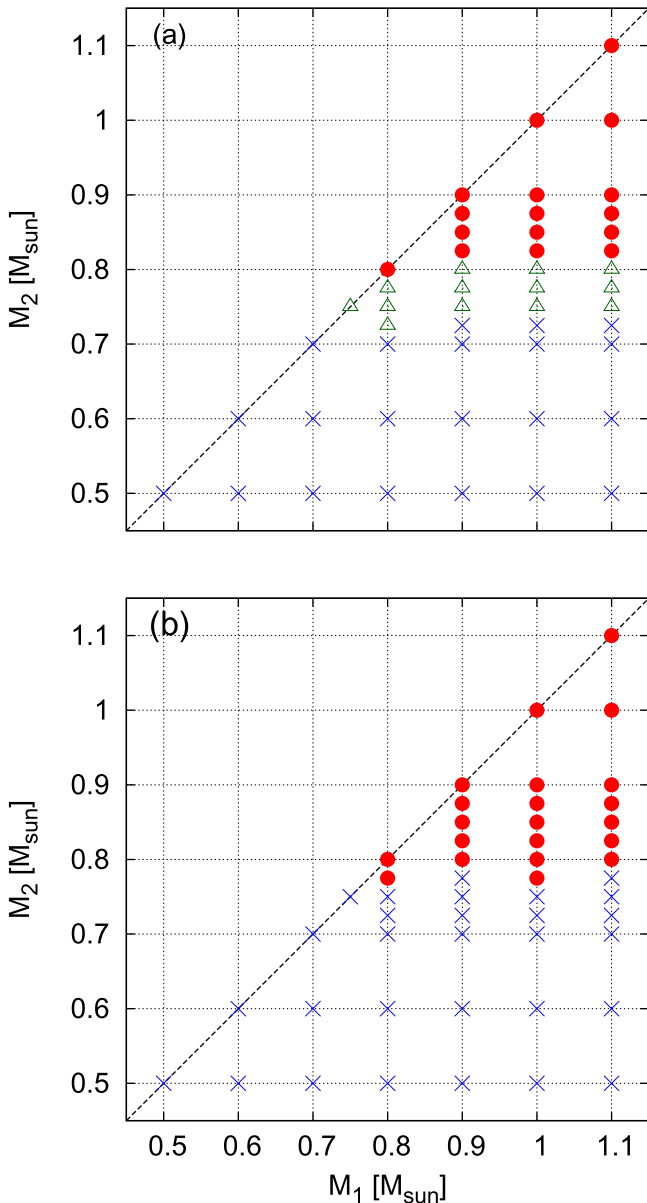


**Figure 10.** Same as Figure 4, but for the case with nuclear burning. The filled circles and crosses have the same meanings as those in Figure 4. Green triangles indicate the mass combinations which satisfy the detonation condition with carbon burning, although they do not satisfy the detonation condition without carbon burning. (a) The results based on our detonation condition in Section 3.2. (b) The results based on the detonation condition of Seitenzahl et al. (2009).

particle which has the highest temperature in the case of  $0.9 + 0.8 M_{\odot}$ . This calculation was done for a period in which carbon burning continued. The red lines indicate the case with the  $\alpha$ -chain reaction network, while green lines indicate the case with only carbon burning. Because we find essentially no difference between them, our simulations including only carbon burning are appropriated to estimate the effect of nuclear burning, and being consistent with the previous studies using  $\alpha$ -chain networks (Pakmor et al. 2010, 2011, 2012b; Raskin et al. 2012), at least until the initiation of detonation.

Thus, the inclusion of carbon burning lowers  $q_{\text{cr}}$  to realize violent merger-induced explosions if we use the same criterion as in Section 3.2. In Figure 10(a), the green triangles are the

models which satisfy our detonation condition with carbon burning, although they do not satisfy the condition without. However, our detonation condition in Section 3.2 is considered under the situation without nuclear burning, so it would no longer be valid in the case with carbon burning. Therefore, for comparison with the results of Pakmor et al. (2011), we adopt the same detonation condition as theirs, i.e., the detection of particles having  $\rho > 2 \times 10^6 \text{ g cm}^{-3}$  and  $T > 2.5 \times 10^9 \text{ K}$  (Seitenzahl et al. 2009). The results are presented in Figure 10(b). Although the boundary of Figure 10(b) is slightly lower than that of Figure 4, the difference between them is small. Thus, we confirm that the detonation condition adopted in Section 3.1 is plausible for the case without nuclear reactions.

The approximated lines of  $q_{\text{cr}}(M_1)$  in the case with carbon burning are also presented in Figure 5, where the red (blue) dashed line indicates an upper (lower) bound. The value of  $q_{\text{cr}}$  with carbon burning is slightly lower than that without carbon burning. The lower bound without carbon burning is almost the same as the upper bound with carbon burning, so we adopt the boundary of Equation (4). Then, our  $q_{\text{cr}}$  is more stringent than that derived in Pakmor et al. (2011). This difference mainly comes from the initial condition as discussed in Section 4.1.

#### 4.4. The Brightness Distribution in Violent Merger Scenarios

Using the results of Pakmor et al. (2011) and the binary population synthesis calculation (Ruiter et al. 2011), Ruiter et al. (2013) estimated the brightness distribution of SNe Ia arising from the violent merger scenario. They adopted the value of  $q_{\text{cr}} = 0.8$  for  $M_1 = 0.9 M_{\odot}$  from Pakmor et al. (2011), and assumed

$$q_{\text{cr}} = \min \left[ 0.8 \left( \frac{M_1}{0.9 M_{\odot}} \right)^{-\eta}, 1.0 \right], \quad (5)$$

where they used  $\eta = 0.0, 0.75, 1.5$ . We add these three lines in Figure 5. Our  $q_{\text{cr}}(M_1)$  is basically more stringent than Ruiter et al. (2013)'s assumptions.

In order to examine how our  $q_{\text{cr}}(M_1)$  would affect the brightness distribution of the violent merger scenario, we adopt the same assumptions as in Ruiter et al. (2013) except for  $q_{\text{cr}}(M_1)$ . For the primary at the time of merging, we use the same WD mass distribution as Ruiter et al. (2013; see also Ruiter et al. 2011), although it is highly uncertain whether the WD can increase its mass by avoiding the formation of a common envelope during the very rapid accretion from the He star companion. We also assume the same  $m_{\text{WD}}-M_{\text{bol}}$  relation of SNe Ia as Ruiter et al. (2013; see Figure 4 in Ruiter et al. 2013; Sim et al. 2010) and a flat mass ratio distribution of DD systems for simplicity. Using either our critical mass ratio or theirs, we calculated the brightness distribution and compared them with each other (Figure 11). We find that there is no significant difference between them qualitatively. This result implies that the  $q_{\text{cr}}$  of the violent merger-induced explosion is not so crucial for the brightness distribution of SNe Ia, as mentioned in Ruiter et al. (2013). Our results are closest to the  $\eta = 1.5$  case among Ruiter et al.'s three cases. In the cases of our  $q_{\text{cr}}$  and Ruiter et al.'s  $\eta = 1.5$ , the brightness distribution concentrates around  $-19.0$  mag. In Figure 11, we add the observational volume-limited brightness distributions of SNe Ia. One in panel (a) is derived by the Lick Observatory Supernova Search (LOSS; Li et al. 2011), and the other in panel (b) is obtained by ROTSE-IIIb (see Table 1 in Quimby

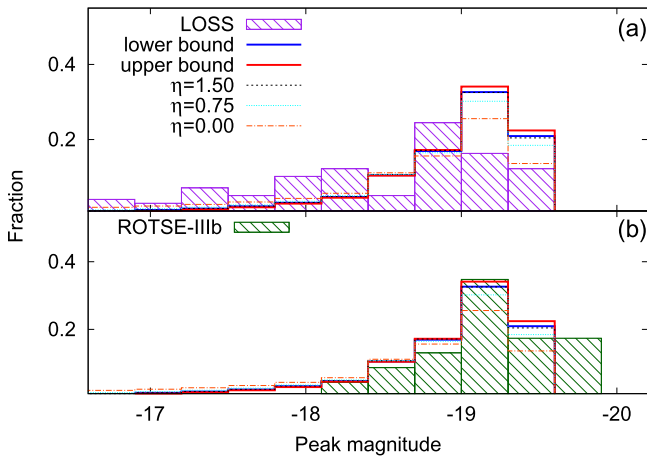


**Figure 11.** SN Ia brightness distributions derived from the present results and those of Ruiter et al. (2013) are compared with the observations. A blue (red) histogram depicts the result calculated from the lower (upper) bound of our  $q_{\text{cr}}$ . Black, cyan, and orange histograms are derived from hypothetical  $q_{\text{cr}}$  values of Ruiter et al. (2013). The hatched purple histogram in panel (a) is a volume-limited brightness distribution derived by LOSS (Li et al. 2011), while the hatched green histogram in panel (b) is that obtained by ROTSE-IIIb (Quimby et al. 2012). Magnitudes of models are bolometric, while those of LOSS and ROTSE-IIIb are in the  $R$  band.

et al. 2012). The fraction of faint events in our models is lower than the observation of LOSS. This discrepancy might decrease if we consider the viewing angle effects (see also the discussion in Ruiter et al. 2013), which might be increasingly important especially for a large value of  $q_{\text{cr}}$ . On the other hand, the results of ROTSE-IIIb are consistent with ours, except most luminous ( $\lesssim -19.5$  mag) events. It should be noted, however, that there are large uncertainties for the observational brightness distribution (e.g., Quimby et al. 2012) and our models are too simple to be compared with the observational results. More detailed studies are required to reach a definitive conclusion.

As the mass ratio is approaching unity, the primary is more strongly deformed by the secondary at merging. As a result, the central density of the primary becomes lower. Because the nucleosynthesis in SN Ia explosions is so sensitive to the density profile near the center of the primary in the violent merger scenario, the amount of  $^{56}\text{Ni}$  decreases as the deformation of the primary becomes higher (Pakmor et al. 2010, 2011). Since our  $q_{\text{cr}}$  is higher than that in the previous studies, the amount of  $^{56}\text{Ni}$  in the violent merger scenario would decrease, while these effects are not included in our brightness estimates.

#### 4.5. The Outcome of Mergers and the Final Fate of Henize 2-428

We summarize the final fates of CO WD mergers in the total mass versus mass ratio (Figure 12), as well as in the mass ratio versus primary mass diagram (Figure 13). The black dotted line shows the line of  $M_{\text{tot}} = M_1 + M_2 = M_{\text{ig}} = 1.38 M_{\odot}$ . If the total mass does not exceed this value, the merger remnant becomes a WD without exploding as an SN Ia (Nomoto et al. 1984).

The direct outcome is a violent merger-induced explosion (VM) in the red hatched region. We adopt Equation (4) as the boundary of this immediate explosion. In other regions, our condition for the violent merger scenario is not satisfied and the merger remnant reaches a quasi-stationary state.

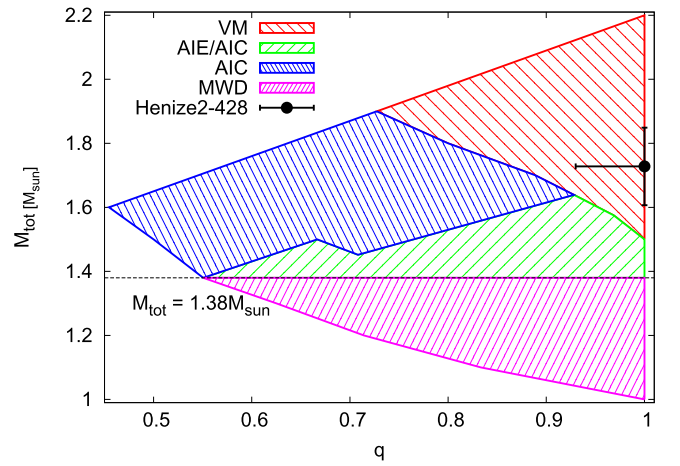


**Figure 12.** Final outcomes of our merger simulations in the total mass vs. mass ratio diagram. We adopt Equation (4) as the boundary between the VM and AIC or AIE/AIC. The boundary between the AIE/AIC and AIC is derived from Sato et al. (2015). The blank (white) regions are where the mass of a WD is  $< 0.5 M_{\odot}$  (He WD region) or  $> 1.1 M_{\odot}$  (ONeMg WD region). He and ONeMg WDs are not the subject of the present study. The black dotted line represents  $M_{\text{tot}} = M_1 + M_2 = M_{\text{ig}} = 1.38 M_{\odot}$ . If the total mass does not exceed this value, the merger remnant becomes a WD without exploding as an SN Ia (Nomoto et al. 1984). The black point shows the possible ranges of the mass ratio and total mass of the central system of Henize 2-428. The parameters of Henize 2-428 are in the region of VM, although we consider the errors. See the text for more details.

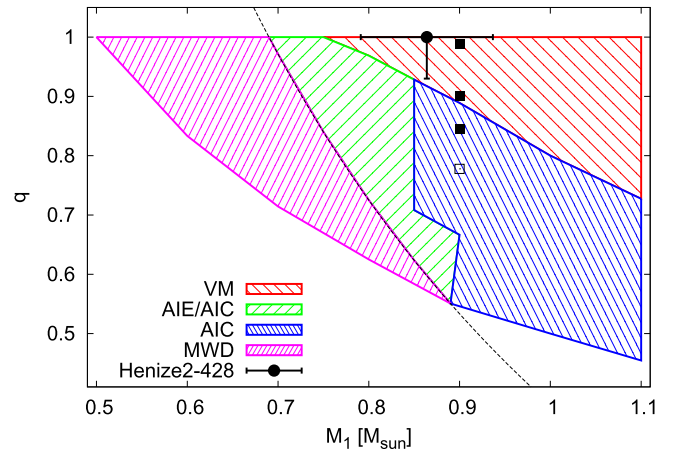


**Figure 13.** Same as Figure 12, but in the mass ratio vs. primary mass diagram. Black squares denote the models calculated by Pakmor et al. (2011). Filled squares indicate the models which satisfy the detonation condition of Seitenzahl et al. (2009), while an open square indicates the model that does not.

The merger remnant consists of three parts, a cold core, hot envelope, and an outer disk (e.g., Benz et al. 1990). In the blue hatched region, off-center carbon burning occurs in the hot envelope (see, e.g., Sato et al. 2015) and the core of the merger remnant would be converted to an oxygen–neon–magnesium (ONeMg) WD (Saio & Nomoto 1985, 1998, 2004). Because the total mass exceeds  $M_{\text{ig}}$ , the merger remnant finally collapses to a neutron star, i.e., the accretion induced collapse (AIC; e.g., Nomoto & Kondo 1991).

In the green hatched region, the core of the merger remnant remains a CO WD because off-center carbon burning does not occur in the early remnant phase ( $10^2$ – $10^3$  s after the secondary is completely disrupted; e.g., Sato et al. 2015). Further evolution of the merger remnant depends on the viscosity and the accretion of material from the outer Keplerian disk

(Yoon et al. 2007). If the viscous heating is sufficiently large in the viscous evolution phase ( $10^4$ – $10^8$  s, e.g., Mochkovitch & Livio 1989), or if the accretion rate exceeds the critical rate of  $\sim 2 \times 10^{-6} M_{\odot} \text{ yr}^{-1}$  in the thermal evolution phase ( $10^5$ – $10^6$  year, e.g., Nomoto & Iben 1985; Yoon et al. 2007), off-center carbon burning is ignited. The final result would be AIC. On the other hand, if the viscous heating is too small or if the accretion rate does not exceed the critical rate, the mass of the merger remnant could grow to exceed  $M_{\text{ig}}$  without off-center carbon burning. We should note that  $M_{\text{ig}}$  of the rotating CO WD is larger than  $1.38 M_{\odot}$  because of the centrifugal force, which is  $1.43 M_{\odot}$  if the rotation is uniform (or larger if differential rotation). Eventually, the merger remnant would explode or collapse depending on  $M_{\text{tot}}$  and the timescale of the angular momentum loss from the merger remnant (Benvenuto et al. 2015). We call the case of explosion the accretion induced explosion (AIE). Because of the above uncertainties, we indicate the green hatched region as AIE/AIC in Figure 12. The boundary between the AIC and AIE/AIC is derived from the results of Sato et al. (2015).

In the magenta hatched region, because off-center carbon burning does not occur and the total mass of the merger remnant does not exceed  $M_{\text{ig}}$ , it possibly leaves a massive CO WD (MWD). Outer boundaries are set from the WD mass range ( $0.5 \sim 1.1 M_{\odot}$ ).

Figures 12 and 13 could not be conclusive. If higher numerical resolutions are applied, the VM region in Figures 12 and 13 would extend downward. As mentioned in Section 4.1, the initial condition of simulations also affects the merger outcomes. If we adopt non-synchronously spinning systems as initial conditions, the VM and AIC region might extend (e.g., Dan et al. 2011; Sato et al. 2015).

In Figure 13, we depict the results of previous works for comparison. The squares indicate the models calculated by Pakmor et al. (2011). Their WD masses are  $M_2 = 0.70, 0.76, 0.81$ , and  $0.89 M_{\odot}$  for  $M_1 = 0.9 M_{\odot}$  (Pakmor et al. 2011). The filled squares are the models which satisfy the detonation condition of Seitenzahl et al. (2009), while the open one did not. Their results indicate that  $q_{\text{cr}} \sim 0.8$  for  $M_1 = 0.9 M_{\odot}$ . Note that our boundary is  $q_{\text{cr}} \sim 0.9$  for  $M_1 = 0.9 M_{\odot}$ , which is more stringent than theirs.

We discuss the final fate of Henize 2-428 on the basis of our results. Henize 2-428 is a bipolar PN and its central system was identified as a binary (e.g., Rodríguez et al. 2001). Santander-García et al. (2015) analyzed the light curve and spectra of the central system. From the depth of the light curve minima, the intensities of two He II 541.2 nm absorption lines, and the obtained radial velocity amplitudes, they interpreted the central system of Henize 2-428 as a DD (double post-AGB core) system with nearly equal masses and effective temperatures. They estimated the total mass of the central system as  $1.76 M_{\odot}$ , which clearly exceeds the Chandrasekhar limit. They also derived the merging time of this system as  $\sim 700$  Myr from the orbital period of 0.176 days. If their interpretation is correct, the central system of Henize 2-428 is the first detected super-Chandrasekhar DD system, which is a candidate of SN Ia progenitors in the DD scenario. Because the mass ratio is close to unity, it likely leads to an SN Ia in the violent merger scenario.

Santander-García et al. (2015) fixed the mass ratio of the central system of Henize 2-428 at unity based on the similar depths of light curve minima and the radial velocity

amplitudes. In this paper, considering  $1\sigma$  uncertainties mentioned in Santander-García et al. (2015), we derive possible ranges of the mass ratio and primary mass without fixing the mass ratio. In Figures 12 and 13, the black point with error bars depicts the possible ranges of the mass ratio and primary mass thus derived. Even considering the uncertainties of the mass ratio and primary mass, we regard that Henize 2-428 is a possible progenitor of SN Ia in the violent merger scenario.

## 5. SUMMARY

We summarize our main results as follows:

(1) Based on the SPH simulations of merging CO WDs, we derived the critical mass ratio for the violent merger scenario, i.e., the  $q_{\text{cr}}$  versus  $M_1$  relation, and compared our result with previous studies. Our  $q_{\text{cr}}(M_1)$  is more stringent than that derived by Pakmor et al. (2011). We conclude that this small difference stems mainly from the differences in the initial condition (whether or not synchronously spinning).

(2) We confirmed that the difference in the critical mass ratio does not significantly affect the brightness distribution of SNe Ia, as claimed in Ruiter et al. (2013). Our results are close to that of the  $\eta = 1.5$  case in Ruiter et al. (2013) and are consistent with the observational result obtained by ROTSE-IIIb (Quimby et al. 2012). Our larger  $q_{\text{cr}}$  would also decrease the relative rate of higher central density primary WDs at the merger, and as a result the total amount of  $^{56}\text{Ni}$  synthesized in the violent merger would be reduced.

(3) We also summarized the direct outcome of CO WD mergers and their final fates in the diagram of  $M_{\text{tot}}$  versus  $q$  (and  $q$  versus  $M_1$ ). On the basis of this diagram, we discussed the fate of the central system of the bipolar PN Henize 2-428, which was recently suggested to be a possible super-Chandrasekhar DD system merging in a timescale much shorter than the Hubble time. Even considering uncertainties of the proposed system in the  $M_{\text{tot}}$  versus  $q$  diagram, we identify the final fate of this system as almost certainly an SN Ia in the violent merger scenario.

We thank the anonymous referee for many detailed comments which helped to improve the paper. Simulations in this paper were performed by using computational resources of Kavli Institute for the Physics and Mathematics of the universe (IPMU), and HA-PACS at the Center for Computational Sciences in University of Tsukuba under the Interdisciplinary Computational Science Program. This research has been supported in part by Grants-in-Aid for Scientific Research (23224004, 23540262, 23740141, 24540227, 26400222, and 26800100) from the Japan Society for the Promotion of Science and by the World Premier International Research Center Initiative, MEXT, Japan. This work is partly supported by the MEXT program for the Development and Improvement for the Next Generation Ultra High-Speed Computer System under its Subsidies for Operating the Specific Advanced Large Research Facilities.

## REFERENCES

- Benvenuto, O. G., Pane, J. A., Nomoto, K., Kitamura, H., & Hachisu, I. 2015, *ApJL*, 809, L6
- Benz, W., Cameron, A. G. W., Press, W. H., & Bowers, R. L. 1990, *ApJ*, 348, 647
- Brown, P. J., Dawson, K. S., Harris, D. W., et al. 2012, *ApJ*, 749, 18
- Cao, Y., Kulkarni, S. R., Howell, D. A., et al. 2015, *Nature*, 521, 328



- Dan, M., Rosswog, S., Brüggen, M., & Podsiadlowski, P. 2014, *MNRAS*, **438**, 14
- Dan, M., Rosswog, S., Guillochon, J., & Ramirez-Ruiz, E. 2011, *ApJ*, **737**, 89
- Dan, M., Rosswog, S., Guillochon, J., & Ramirez-Ruiz, E. 2012, *MNRAS*, **422**, 2417
- D’Souza, M. C. R., Motl, P. M., Tohline, J. E., & Frank, J. 2006, *ApJ*, **643**, 381
- Eggleton, P. P. 1983, *ApJ*, **268**, 368
- Foley, R. J., Challis, P. J., Filippenko, A. V., et al. 2012, *ApJ*, **744**, 38
- Frew, D. J., Parker, Q. A., & Bojicic, I. S. 2015, *MNRAS*, **455**, 1459
- Fryer, C. L., Ruiter, A. J., Belczynski, K., et al. 2010, *ApJ*, **725**, 296
- Fuller, J., & Lai, D. 2014, *MNRAS*, **444**, 3488
- García-Berro, E., Soker, N., Althaus, L. G., Ribas, I., & Morales, J. C. 2015, *NewA*, **45**, 7
- Gingold, R. A., & Monaghan, J. J. 1982, *JCoPh*, **46**, 429
- González Hernández, J. I., Ruiz-Lapuente, P., Tabernero, H. M., et al. 2012, *Natur*, **489**, 533
- Guerrero, J., García-Berro, E., & Isern, J. 2004, *A&A*, **413**, 257
- Guillochon, J., Dan, M., Ramirez-Ruiz, E., & Rosswog, S. 2010, *ApJL*, **709**, L64
- Hillebrandt, W., & Niemeyer, J. C. 2000, *ARA&A*, **38**, 191
- Iben, I., Jr., & Tutukov, A. V. 1984, *ApJS*, **54**, 335
- Kashyap, R., Fisher, R., García-Berro, E., et al. 2015, *ApJL*, **800**, L7
- Kerzendorf, W. E., Schmidt, B. P., Laird, J. B., et al. 2012, *ApJ*, **759**, 7
- Kobayashi, C., Tsujimoto, T., Nomoto, K., Hachisu, I., & Kato, M. 1998, *ApJL*, **503**, L155
- Li, W., Leaman, J., Chornock, R., et al. 2011, *MNRAS*, **412**, 1441
- Lorén-Aguilar, P., Isern, J., & García-Berro, E. 2009, *A&A*, **500**, 1193
- Maoz, D., Mannucci, F., & Nelemans, G. 2014, *ARA&A*, **52**, 107
- Marion, G. H., Brown, P. J., Vinkó, J., et al. 2015, arXiv:1507.07261
- McCully, C., Jha, S. W., Foley, R. J., et al. 2014, *Natur*, **512**, 54
- Mochkovitch, R., & Livio, M. 1989, *A&A*, **209**, 111
- Moll, R., Raskin, C., Kasen, D., & Woosley, S. E. 2014, *ApJ*, **785**, 105
- Monaghan, J. J. 2005, *RPPh*, **68**, 1703
- Motl, P. M., Frank, J., Tohline, J. E., & D’Souza, M. C. R. 2007, *ApJ*, **670**, 1314
- Nakasato, N., Ogiya, G., Miki, Y., Mori, M., & Nomoto, K. 2012, arXiv:1206.1199
- Nomoto, K. 1982, *ApJ*, **257**, 780
- Nomoto, K., & Iben, I., Jr. 1985, *ApJ*, **297**, 531
- Nomoto, K., & Kondo, Y. 1991, *ApJL*, **367**, L19
- Nomoto, K., Thielemann, F. K., & Yokoi, K. 1984, *ApJ*, **286**, 644
- Olling, R. P., Mushotzky, R., Shaya, E. J., et al. 2015, *Natur*, **521**, 332
- Pakmor, R., Edelmann, P., Röpke, F. K., & Hillebrandt, W. 2012a, *MNRAS*, **424**, 2222
- Pakmor, R., Hachinger, S., Röpke, F. K., & Hillebrandt, W. 2011, *A&A*, **528**, A117
- Pakmor, R., Kromer, M., Röpke, F. K., et al. 2010, *Natur*, **463**, 61
- Pakmor, R., Kromer, M., Taubenberger, S., et al. 2012b, *ApJL*, **747**, L10
- Pakmor, R., Kromer, M., Taubenberger, S., & Springel, V. 2013, *ApJL*, **770**, L8
- Perlmutter, S., Aldering, G., Goldhaber, G., et al. 1999, *ApJ*, **517**, 565
- Quimby, R. M., Yuan, F., Akerlof, C., Wheeler, J. C., & Warren, M. S. 2012, *AJ*, **144**, 177
- Rasio, F. A., & Shapiro, S. L. 1995, *ApJ*, **438**, 887
- Raskin, C., Kasen, D., Moll, R., Schwab, J., & Woosley, S. E. 2014, *ApJ*, **788**, 75
- Raskin, C., Scannapieco, E., Fryer, C., Rockefeller, G., & Timmes, F. X. 2012, *ApJ*, **746**, 62
- Riess, A. G., Filippenko, A. V., Challis, P., et al. 1998, *AJ*, **116**, 1009
- Rodríguez, M., Corradi, R. L. M., & Mampaso, A. 2001, *A&A*, **377**, 1042
- Rosswog, S. 2009, *NewAR*, **53**, 78
- Ruiter, A. J., Belczynski, K., Sim, S. A., et al. 2011, *MNRAS*, **417**, 408
- Ruiter, A. J., Sim, S. A., Pakmor, R., et al. 2013, *MNRAS*, **429**, 1425
- Saio, H., & Nomoto, K. 1985, *A&A*, **150**, L21
- Saio, H., & Nomoto, K. 1998, *ApJ*, **500**, 388
- Saio, H., & Nomoto, K. 2004, *ApJ*, **615**, 444
- Santander-García, M., Rodríguez-Gil, P., Corradi, R. L. M., et al. 2015, *Natur*, **519**, 63
- Sato, Y., Nakasato, N., Tanikawa, A., et al. 2015, *ApJ*, **807**, 105
- Schaefer, B., & Pagnotta, A. 2012, *Natur*, **481**, 164
- Segretain, L., Chabrier, G., & Mochkovitch, R. 1997, *ApJ*, **481**, 355
- Seitenzahl, I. R., Meakin, C. A., Townsley, D. M., Lamb, D. Q., & Truran, J. W. 2009, *ApJ*, **696**, 515
- Sim, S. A., Röpke, F. K., Hillebrandt, W., et al. 2010, *ApJL*, **714**, L52
- Tanikawa, A., Nakasato, N., Sato, Y., et al. 2015, *ApJ*, **807**, 40
- Timmes, F. X. 1999, *ApJS*, **124**, 241
- Timmes, F. X., & Swesty, F. D. 2000, *ApJS*, **126**, 501
- Webbink, R. F. 1984, *ApJ*, **277**, 355
- Yoon, S. C., Podsiadlowski, P., & Rosswog, S. 2007, *MNRAS*, **380**, 933
- Zhu, C., Chang, P., van Kerkwijk, M. H., & Wadsley, J. 2013, *ApJ*, **767**, 164